

DEVELOPMENT OF A PASS-THROUGH DIAGNOSTIC FOR NEXT-GENERATION XFELs USING DIAMOND SENSORS*

I. Silva Torrecilla[†], B. Jacobson, J. MacArthur, D. Zhu

SLAC National Accelerator Laboratory, Menlo Park, California, USA

J. Bohon, D. Kim, J. Smedley, Los Alamos National Laboratory, Los Alamos, New Mexico, USA

E. Gonzalez, S. Kachiguine, F. Martinez-Mckinney, S. Mazza, M. Nizam, N. Norvell, R. Padilla,

E. Potter, E. Ryan, B. Schumm, M. Tarka, M. Wilder, Santa Cruz Institute for Particle Physics and the University of California at Santa Cruz, Santa Cruz, California, USA

C. T. Harris, Sandia National Laboratory, Albuquerque, New Mexico, USA

Abstract

X-ray FELs deliver rapid pulses on the femtoseconds scale, and high peak intensities that fluctuate strongly on a pulse-to-pulse basis. The fast drift velocity, and high radiation tolerance properties of CVD (chemical vapor deposition) diamonds, make these crystals a good candidate material for developing a multi-hundred MHz pass-through diagnostic for the next generation of XFELs. Commercially available diamond sensors work as position-sensitive pass-through diagnostics for nJ-level pulses from synchrotrons. Supported by the University of California and the SLAC National Laboratory, a collaboration of UC campuses and National Laboratories have developed a new approach to the readout of diamond diagnostic sensors designed to facilitate operation for FEL-relevant uJ and mJ pulses. Single-crystal diamond detectors have been tested on the XPP end station of the Linac Coherent Light Source beam at SLAC. We present results on the linearity and charge collection characteristics as a function of the density of deposited charge.

INTRODUCTION

Monocrystalline diamonds are recognized to exhibit a number of properties that make them attractive options for a broad range of sensor applications. Superior radiation tolerance, a fast saturated drift velocity (approximately 200 $\mu\text{m}/\text{nsec}$) and superior thermal conductivity (2200 W/m-K) distinguish diamond among other semiconductor sensor materials such as silicon and gallium-arsenide.

Here, we explore the use of diamond sensors as a pass-through diagnostic for X-ray Free Electron Laser (XFEL) beams. For this application, involving intense X-ray beams being trained directly on the diagnostic sensor, diamond properties that might be disadvantageous for other applications provide additional advantages relative to other sensor materials. The low atomic number of carbon leads to a relatively small scattering cross section for X-ray above the carbon K-shell edge of 0.28 keV, limiting the absorption of

the XFEL beam as it passes through the diagnostic. In addition, the large diamond band gap of 5.5 eV, and resulting pair excitation energy of 13.3 eV [1], limits the production of signal charge relative to other sensor materials.

In this study, we explored the characteristics of diamond-sensor charge collection in limits relevant to their application as pass-through diagnostics for high-intensity, high repetition-rate X-ray beams. These studies were performed at the XPP beamline of the Linac Coherent Light Source (LCLS) at the SLAC National Accelerator Laboratory on April 5-6, 2021. The studies made use of a monochromatic beam of 11.89 keV X-rays with individual pulse varying in energy from 1 μJ to nearly 100 μJ . Both the duration and efficiency of charge collection were studied as a function of the density of deposited charge within the diamond sensor.

SENSOR AND READOUT

The studies made use of a 4x4 mm² monocrystalline diamond substrate, provided by the Element Six corporation and thinned by Applied Diamond, Inc. The diamond was plated with planar platinum electrodes of area approximately 3.5x3.5 mm² and 25 nm thickness at the Center for Integrated Nanotechnologies (CINT) facility in Albuquerque, New Mexico, USA. The thickness of the diamond substrate was measured to be $37 \pm 10 \mu\text{m}$ in the laboratory of the Santa Cruz Institute for Particle Physics (SCIPP) on the campus of the University of California at Santa Cruz.

The sensor was mounted on a printed-circuit board (PCB), produced by the SCIPP laboratory, featuring a low-impedance signal path designed to circulate large amounts of signal charge at high bandwidth. Figure 1 shows the details of the PCB signal path, including the loaded diamond sensor described above. To reduce inductive load associated with bond wires, the sensor is connected to the readout path through a metallic band composed of indium. This band carries signal charge to a series array of two resistors – a 1 Ω resistor followed by a 10 m Ω resistor, with contacts on the long side to minimize inductance – that shunt the signal current directly to ground. 50 Ω pick-off traces make contact with the sensor side of both the 1 Ω and 10 m Ω resistors, each of which terminates at an SMA connector close to the pickoff point, providing signals that can be digitized and recorded with a high-bandwidth digital storage oscilloscope. Figure 2 provides a larger-scale view of

* Work supported by the UC-National Laboratory Fees Research Program grant ID #LFR-20-653232, the U.S. Department of Energy, grant number DE-SC0010107 (SCIPP), contract 89233218CNA000001 (LANL), Contract DE-NA-0003525 (Sandia), Contract No. DE-AC02-76SF00515(SLAC).

[†] email address isleydys@slac.stanford.edu

the PCB, showing the signal-trace paths and SMA connector footprints. The AC signal return path is provided by a bank of 44 parallel 22 μF capacitors, amounting to a total capacitance of approximately 1 mF, between ground and the bias plane onto which the sensor is attached making use of Leitsilber Conductive Silver Cement. The redundant parallel paths reduce the overall inductance of the signal return path, while the large capacitance provides an ample reservoir of charge to support the large signal charges generated by the intense XFEL pulse.

It should be noted that the charge collection speed can be very fast for the sensor described above and shown in Fig. 1. With a saturated drift speed in diamond of approximately 200 $\mu\text{m}/\text{nsec}$, absent effects from space-charge and electronic impedance, the nominal charge collection time for the 37 μm thick sensor is less than 200 psec.

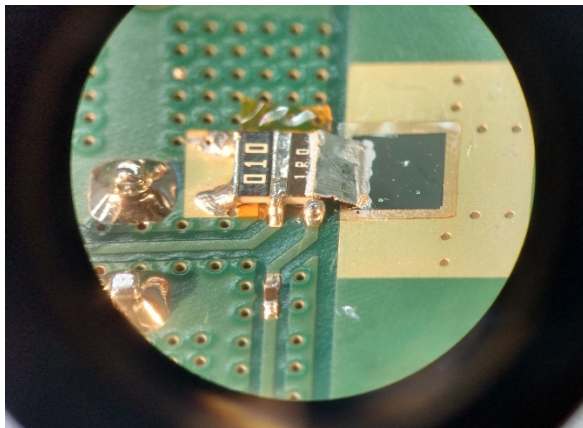


Figure 1: Detail of the readout PCB signal path showing the 37 μm thick diamond sensor, the low-impedance indium band connecting the sensor to the readout network, the series array of 1 Ω and 10 m Ω resistors that shunt the signal to ground, and the two 50 Ω pick-off traces.

DATA ACCUMULATION

The data used in this study was accumulated in the early morning of April 6, 2021. The monochromatized LCLS beam provided pulses of 11.89 keV X-rays with a falling energy spectrum (see Fig. 3) that ranged between 1 and 80 μJ . Making use of energy-attenuation coefficients from [2], approximately 1.3% of the beam energy was absorbed by the sensor as the pulse passed through it.

Data was accumulated with both the full beam as well as with a beam attenuated by 90% through the insertion of a physical attenuator upstream of the sensor assembly. The two signal pick-offs (1 Ω and 10 m Ω) were read out by a 25 GHz digital storage oscilloscope operating with a sampling rate of 40 Gs/S. High-bandwidth signal-path attenuation was used, as needed, to ensure that the pulses didn't saturate the dynamic range of the oscilloscope. Beam was provided both in un-focused (FWHM estimated to be 350 μm) and focused (FWHM estimated to be 43 μm) modes. Data were taken for sensor bias voltage ranging between 5.4 and 100 Volts. For each configuration of beam intensity, beam focus and bias voltage, runs of approximately 1000 pulses were accumulated. The signals from

the 10 m Ω signal pick-off were found to be too noisy to use for the characterization of the detector response, and will not be made use of in the results that follow.

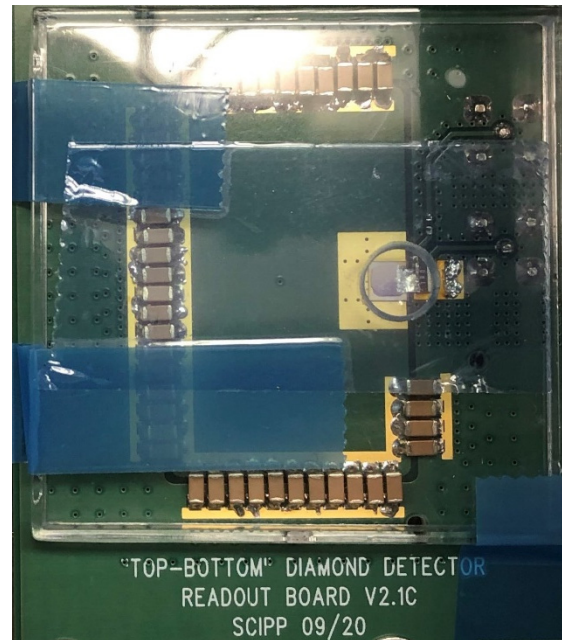


Figure 2: Full view of the readout PCB showing the AC return path provided by a highly parallelized array of 22 μF capacitors. Note that in this photograph, the assembly is rotated by 180 degrees relative to that of Fig. 1.

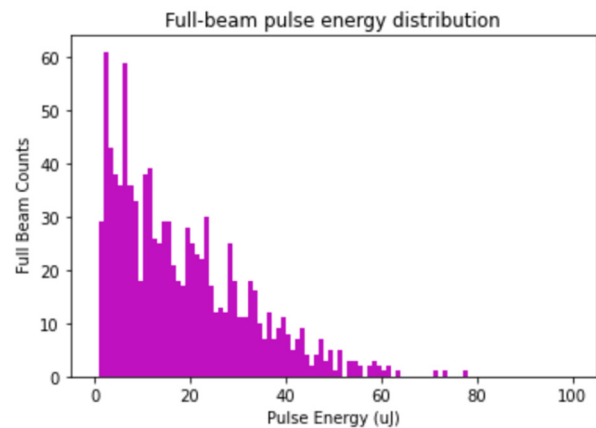


Figure 3: Typical distribution of pulse energies delivered by the LCLS during data accumulation.

ANALYSIS AND RESULTS

Charge collection current was estimated according to

$$I_{coll}(t) = V(t)/R_{eff}$$

where I_{coll} is the estimated charge-collection current, V is the measured signal voltage, and R_{eff} is the effective resistance of the signal path, including both the applicable shunt resistance and the 50 Ω termination resistance of the oscilloscope. For the 1 Ω signal pickoff, this parallel combination of 1.01 Ω and 50 Ω led to an effective resistance of $R_{eff} = 0.99 \Omega$.

Total collected charge, as a function of collection time, was estimated by integrating, for signals within a given pulse-energy bin, the average charge collection current from the point of passage of the beam through the sensor ($t=0$) to the specified collection time:

$$Q_{coll}(t_{coll}) = \int_0^{t_{coll}} I_{coll}(t) dt .$$

Figures 4 and 5 show the collected charge as a function of time, estimated in this way, for signals arising from successive bins in delivered pulse energy, for unfocused and focused beam, respectively. The signals shown are those arising when the diamond sensor was biased to 100 V. In comparing the detector response between the cases of unfocused and focused beam, it should be noted that, in a given pulse energy bin, the total delivered charge is essentially identical; what differs between the two cases is the density of generated charge carriers created inside the diamond bulk, hereafter referred to as the “plasma density” ρ_P .

It is seen that the time required for full collection of the signal charge increases with total delivered charge, but also is significantly larger when, for a given pulse energy, the beam is focused. This suggests that characteristics of the charge collection, such as collection time and collection efficiency, may be characterized in terms of plasma density, a property internal to the diamond sensor itself, independent of the particular scheme employed to extract its signal.

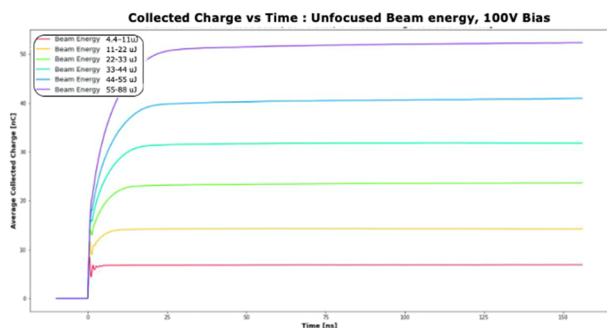


Figure 4: Collected charge as a function of collection time for a sensor bias of 100 V, with the beam focused to a FWHM of 350 μm .

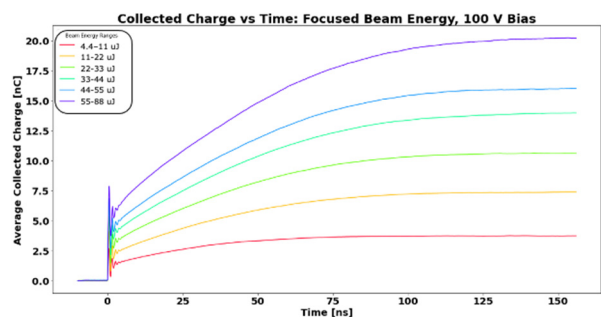


Figure 5: Collected charge as a function of collection time for a sensor bias of 100 V, with the beam focused to a FWHM of 43 μm .

In the following, we estimate plasma density ρ_P according to

$$\rho_P = 0.76 \frac{Q_{dep}}{V}$$

where Q_{dep} is the charge deposited in the diamond bulk and $V = \pi T(d/2)^2$ is the volume occupied by the plasma, with T being the sensor thickness and d equal to the full-width at half-maximum quoted above for the unfocused and focused beams (350 and 43 μm , respectively). The factor of 0.76 represents the fraction of a gaussian beam contained within its FWHM.

The value of Q_{dep} in each pulse-energy bin is estimated by multiplying the mean delivered pulse energy in the given bin by a conversion factor of 0.931 nC/ μJ . This factor is given by the ratio of $Q_{coll}(t \rightarrow \infty)$, the asymptotic value of the observed collected charge estimate, to the mean delivered pulse energy in the lowest pulse-energy bin of the 100%, 100 V bias, unfocused-beam running, for which the charge collection efficiency is assumed to be 100%. This assumption will be justified below.

Making use of this conversion factor, and the expression for plasma density, both the deposited charge and the plasma density can be estimated for any delivered pulse energy for any configuration of the experimental setup. By comparing $Q_{coll}(t \rightarrow \infty)$ with the deposited charge estimate (estimate of the charge generated by the beam passage), an estimate of the charge collection efficiency can be made as a function of plasma density. For the case of 100 V of applied bias, for which both full-energy and 90%-attenuated data was accumulated with unfocused beam, and full-energy data was accumulated for focused beam, the range of plasma density deposited in the sensor varied by nearly four orders of magnitude.

Figure 6 shows the estimated charge collection efficiency as a function of plasma density for the three bias voltages for which data was accumulated for both unfocused and focused beam: 20 V, 60 V and 100 V. The consistency of the estimated charge collection efficiency, albeit with limited statistics, for the 90%-attenuated running, at and below the plasma density associated with the lowest energy bin for the case of unfocused beam, supports the assumption that the charge collection efficiency is near 100% for that data. For the highest bias voltage (100 V, corresponding to a bias field of approximately 2.7 V/ μm), charge collection efficiency loss is observed to occur for plasma densities above 10^{16} cm^{-3} . For the 60 V and 20 V (1.6 and 0.54 V/ μm , respectively) bias running, charge collection efficiency worsens with lessening bias, with efficiency loss observed even for a plasma density as low as 10^{16} cm^{-3} , the lowest density explored for these lesser biases.

From the information shown in Figs 4 and 5, as well as corresponding information for running with sensor biases of 20 V and 60 V, the time required to accumulate a given fraction of the asymptotic value $Q_{coll}(t \rightarrow \infty)$ can be estimated as a function of plasma density. Values of this estimate for a fraction of 95% of $Q_{coll}(t \rightarrow \infty)$ are displayed in

Fig. 7 as a function of plasma density. The charge collection time, characterized in this way, depends strongly upon both plasma density and applied bias field, and approaches 100 ns even for the highest bias field (2.7 V/ μm) explored in this study.

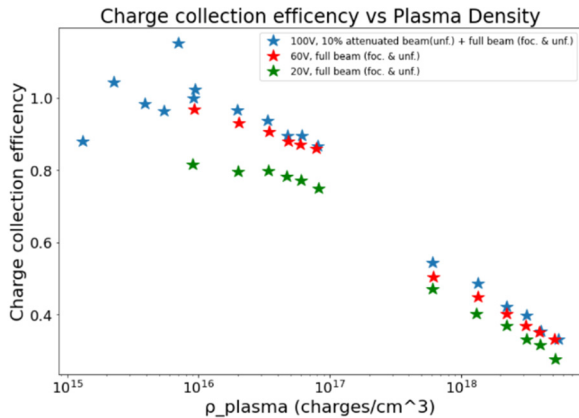


Figure 6: Estimated charge collection efficiency as a function of plasma density (cm^{-3}) for 100 V, 60 V and 20 V sensor bias.

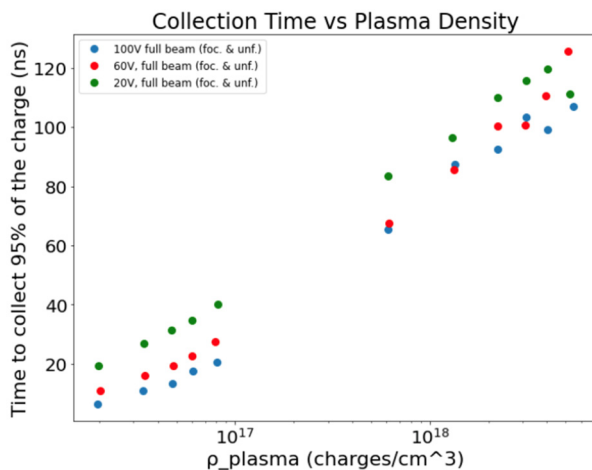


Figure 7: Time required to collect 95% of $Q_{\text{coll}}(t \rightarrow \infty)$, as a function of plasma density, for various detector biasing levels.

SUMMARY AND CONCLUSIONS

In a study to explore its suitability as a pass-through diagnostic for high-intensity X-ray beams, a thin diamond sensor, biased to fields as high as 2.7 V/ μm , was exposed to XFEL pulses of 11.89 keV X-rays with energies of up to 80 μJ . For this highest bias voltage, charge collection efficiency was found to be maintained for plasma densities as high as 10^{16} cm^{-3} , with the charge collection efficiency worsening monotonically with applied bias voltage. Charge collection time, characterized by the amount of time required to accumulate 95% of the asymptotic value of collected charge, was also found to depend strongly on plasma density and detector bias voltage. While the results

suggest that charge collection speed and efficiency may be improved by increasing the bias field above 2.7 V/ μm (the maximum value used in the study), it seems that the intrinsic charge collection properties of monocrystalline diamond will present challenges to the development of pass-through diagnostics for high-intensity XFEL beams (which can approach several mJ), especially for high repetition-rate applications.

ACKNOWLEDGEMENTS

This work was supported by the UC-National Laboratory Fees Research Program grant ID #LFR-20-653232, and by the U.S. Department of Energy, grant number DE-SC0010107. This work was performed, in part, at the Center for Integrated Nanotechnologies, an Office of Science User Facility operated for the U.S. Department of Energy (DOE) Office of Science by Los Alamos National Laboratory (Contract 89233218CNA000001) and Sandia National Laboratories (Contract DE-NA-0003525). We also acknowledge the generous support of the SLAC National Accelerator Laboratory, through its provision of LCLS beam time and staff support. Use of the Linac Coherent Light Source (LCLS), SLAC National Accelerator Laboratory, is supported by the U.S. Department of Energy, Office of Science, Office of Basic Energy Sciences under Contract No. DE-AC02-76SF00515.

REFERENCES

- [1] Jeffrey W. Keister and John Smedley, “Single Crystal Diamond Photodiode for Soft X-ray Radiometry”, *Nucl. Instrum. & Meth. A*, vol. 606, pp. 774-779, 2009.
- [2] <https://physics.nist.gov/PhysRefData/Xray-MassCoef/ElemTab/z06.html>